This peer-reviewed published paper appears as: Motallebi, M., Lignos, D.G. and Rogers, C. (2018). "Behaviour of Stiffened Extended Shear Tab Connections under Gravity Induced Shear Force", *Journal of Constructional Steel Research*, Vol. 148, pp. 336-350, doi: https://doi.org/10.1016/j.jcsr.2018.06.011.

# Behaviour of Stiffened Extended Shear Tab Connections under Gravity Induced Shear Force

Mohammad Motallebi[1], Dimitrios G. Lignos[2], Colin A. Rogers[3]

[1] Graduate Research Assistant, Department of Civil Engineering and Applied Mechanics, McGill University, Montreal, QC. Email: mohammad.motallebinasrabadi@mail.mcgill.ca

[2] Dimitrios G. Lignos, Associate Professor, School of Architecture, Civil and Environmental Engineering, Swiss Federal Institute of Technology, Lausanne (EPFL), Lausanne, Switzerland, Email: dimitrios.lignos@epfl.ch

[3] Corresponding author
Colin A. Rogers, Associate Professor, Department of Civil Engineering and Applied Mechanics, McGill University, Montreal, QC. Email: colin.rogers@mcgill.ca
817 Sherbrooke Street West
Montreal QC, Canada, H3A 0C3
Tel. 514 398-6449
Fax. 514 398-7361

**ABSTRACT**

Stiffened extended shear tab connections (either in full-depth or partial-depth configurations) are widely used to connect simply supported beams to the web of supporting girders or columns. Full-scale laboratory tests of stiffened extended shear tab connections underscored the differences between their observed and expected design strength calculated according to current design specifications. In particular, the design procedure of such connections neglects the influence of the out-of-plane deformation of the supporting girder web on yielding and inelastic buckling of the shear plate. These are the main governing failure modes for the full-depth configurations of stiffened extended shear tabs, when placed on one side of a supporting girder or column. This paper aims to address the effect of the girder web flexibility on the load transfer mechanism and failure modes of extended beam-to-girder shear tab connections. The findings are based on finite element (FE) simulations validated with full-scale experiments on beam-to-girder shear tab connections. The influence of interior versus exterior girder webs on the connection behaviour is assessed. Emphasis is placed on the influence of the girder web deformation and shear tab configuration on the load transfer mechanism and the ultimate strength of extended beam-to-girder connections. The current design practice is evaluated and improved recommendations are provided for the design of full-depth extended beam-to-girder shear tabs.

**Keyword**s: extended shear tab, connection, plate buckling, design, effective eccentricity, finite element simulation

## 1 Introduction

Due to ease of fabrication and erection of extended shear tab connections, they have been widely used in steel construction practice. They consist of a steel plate, which is shop-welded to the supporting girder or column and then bolted to the supported beam in the field. Referring to Fig. 1, the increased shear tab length allows for the beam to be connected to the column or girder web without coping the beam's flanges. The shear plate may be welded to the girder web (i.e. unstiffened configuration, Fig. 1a), or may be connected either to the top flange (i.e. partial-depth stiffened configuration, Fig. 1b) or to both the top and bottom flanges (i.e. full-depth stiffened configuration, Fig. 1c).

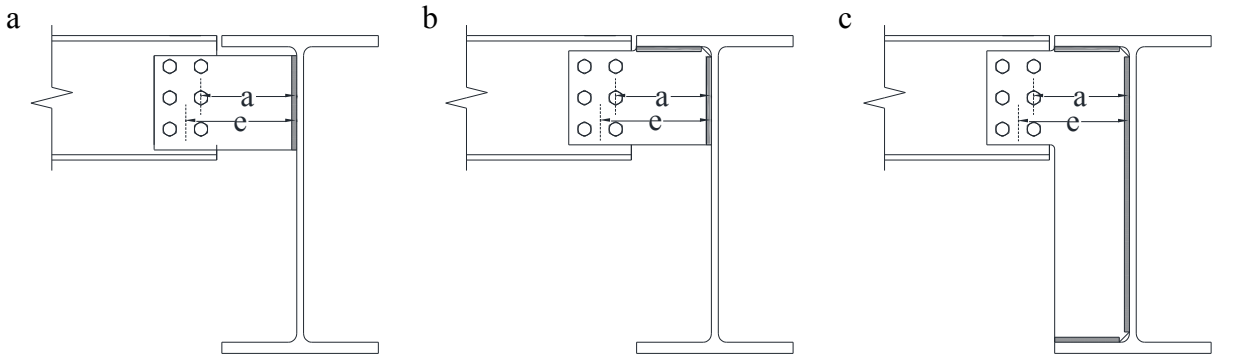


Fig. 1. Extended beam-to-girder shear tab connections: (a) partial-depth unstiffened, (b) partial-depth stiffened, (c) full-depth stiffened

The potential failure modes of unstiffened extended shear tab connections are summarized in the 15$^{h}$ Edition of the AISC Steel Construction Manual [1]. The plate thickness and the weld throat are proportioned to develop plate yielding prior to bolt shear and weld tearing such that a stable connection behaviour can be achieved that provides adequate ductility for the imposed loading. The 15$^{th}$ Edition AISC Steel Construction Manual, [1], uses the rectangular plate buckling model [2,3] to account for the shear plate flexural buckling, while the 14$^{th}$ Edition of the AISC Steel Construction Manual [4] implements equations corresponding to the flexural buckling resistance of a doubly coped beam [5-6].

59 The AISC design method [1] was originally developed for unstiffened extended shear tabs
60 connected to rigid supports. The same method was further applied to unstiffened extended shear
61 tabs connected to flexible supports by considering the out-of-plane deformation of the supporting
62 element's web (either girder or column) as a serviceability issue for the supported beam [7]. The
63 stiffened shear tab may subject the supporting member (girder or column) to higher rotational
64 demands, which are typically not considered in frame analysis. This raises some concerns about
65 the desirability of stiffened extended shear tabs [8]. Nonetheless, practicing structural engineers
66 use extensively the stiffened extended shear tab due to their concern about the stability of either
67 the beam or the shear plate itself. An increase in the thickness of the shear plate may not be an
68 option to address the stability concerns. The reason is that the maximum thickness of the shear
69 plate is limited to ensure yielding prior to shear fracture of the bolts. Further, regardless of the
70 shear tab connection detailing, the column may also need stabilizer plates if a fully restrained
71 beam-to-column moment connection exists in the perpendicular direction (i.e., part of a moment-
72 resisting frame). If the supporting members (either column or girder) are part of the lateral load
73 resisting system, their behaviour under gravity and lateral loads may be adversely affected by a
74 potential out-of-plane deformation of the respective columns and/or girders. This may be
75 particularly concerning in North America when deep members are utilized in the lateral load
76 resisting system [9].

77 Considering the above discussion, it is apparent that there is limited guidance for the design
78 of stiffened extended shear tabs. In the design of extended shear tabs the current AISC Manual [1]
79 suggests considering the inflection point at the face of the supporting member (girder web in this
80 case) (Fig. 2a). Then, the design shear force and flexural moment for the bolt group (Figs. 2b and
81 3a) shall be the shear force at the beam end (R) and the resultant eccentric moment ($M=R \times e$),

respectively. Furthermore, the vertical weld line, which connects the shear plate to the girder web (or the column web as shown in Fig. 3a), is designed to resist the shear force (R) alone. The horizontal weld lines, that connect the shear plate to the girder flanges (the stabilizer plates in Fig. 3a), are not considered as load carrying welds; as such, they are detailed having a minimum size. Of note, Figs. 2b and 3a show the symmetric configuration where the centreline of the supported beams was located midway between the girder flanges (the two stabilizer plates in Fig 3a). This configuration may not be applicable if a supported beam is connected to a deeper supporting girder (Fig. 2c). Further, the symmetric configuration may not be applicable in the presence of continuity plates of a fully restrained moment connection joining a deeper beam to the column orthogonal direction, as illustrated in Fig. 3b.

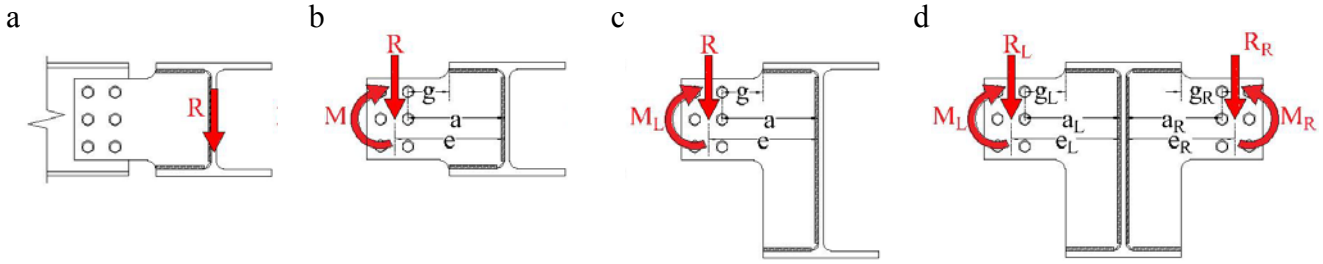


Fig. 2. Full-depth extended beam-to-girder shear tab: (a) location of inflection point, (b) single-sided (the beam and girder have the same depth), (c) single-sided, (d) double-sided

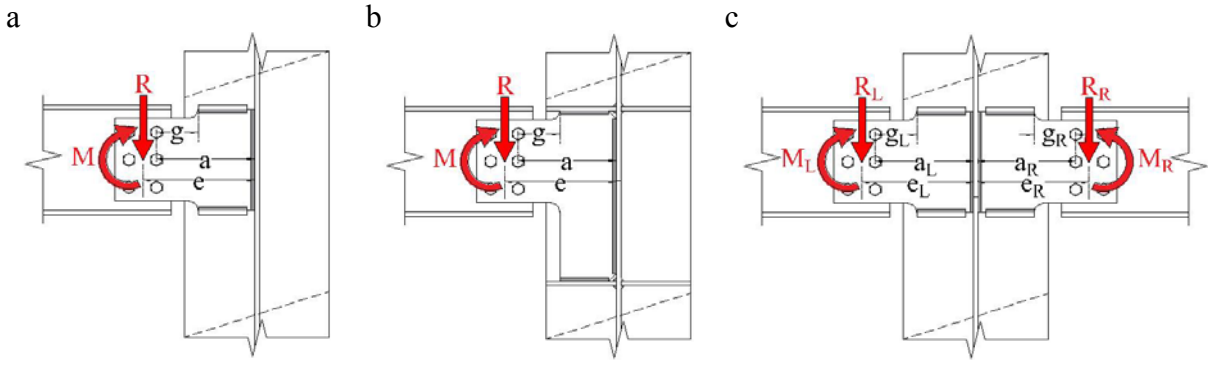


Fig. 3. Extended beam-to-column shear tab with stiffeners: (a) single-sided, (b) single-sided with continuity plates, (c) double-sided

For a girder or column, which supports a beam on each side (Figs. 2d and 3c), each connection is designed for its corresponding shear force ($R_R$ and $R_L$) and a portion of the net flexural moment

98 ($M_R$-$M_L$=$R_R$×$e_R$ - $R_L$×$e_L$) determined based on the engineer's judgement [1]. For the design of
99 other connection elements, i.e. the shear plate and stabilizer plates, the current AISC Manual gives
100 no explicit recommendations.

101 It is often the case that the design of stiffened beam-to-girder shear tabs follows that of the
102 unstiffened ones. This leads to either bolt shear fracture or yielding of the extended portion of the
103 shear plate as the governing failure mode of the stiffened shear tab connection. However, this is
104 not consistent with the observed behaviour of such connections from laboratory tests [10-12].

105 Findings from past experimental and finite element studies [10-13] reveal that bolt shear
106 fracture is not deemed to be critical in the context of the connection configurations that were
107 evaluated. Plate buckling is the governing failure mode for stiffened full-depth configurations of
108 either beam-to-girder [10] or beam-to-column shear tab connections [11, 12]. Notably, in stiffened
109 extended beam-to-girder shear tabs with a partial-depth shear plate, shear plate yielding and
110 twisting were the governing failure modes [10, 13]. Although the girder web mechanism was
111 evident, it was a secondary failure mode that mostly occurred in deep connections i.e. shear tab
112 connections with a single vertical line of six or more bolts [10,13].

113 In order to improve the current design provisions for stiffened extended shear tabs, Fortney
114 and Thornton [14] recommended that the distance between the bolt line and the toe of a stabilizer
115 plate should be used as the bolt group eccentricity for the design of extended shear tabs with
116 stabilizer plates. However, their recommendation was not substantiated with either published
117 laboratory tests or finite element analyses. Although the design calculations based on the
118 aforementioned eccentricity result in a more realistic bolt shear strength prediction, they still
119 overestimate the shear plate buckling strength, which is the governing failure mode observed in
120 laboratory tests [10-12].

121 The test results of extended beam-to-girder shear tabs are limited to a few configurations with
122 a single vertical row of bolts, although shear tabs with multiple bolt lines are common in current
123 steel construction practice. Multiple bolt lines may decrease the shear plate buckling strength
124 because the shear plate is loaded farther from its support, the weld line. Furthermore, most of the
125 experimental studies on stiffened beam-to-column shear tabs [12] were limited to the configuration
126 similar to that shown in Fig. 3a. Nevertheless, this configuration would need to be modified if
127 continuity plates were incorporated into a fully restrained beam-to-column connection (Fig. 3b).
128 As such, conflicting opinions exist regarding the design and testing of shear tab connections as to
129 the design of stiffened extended shear tabs, and the definition of the eccentric loading.

130 To further our understanding on how extended shear tab connections behave under gravity-
131 induced shear forces, a research program was carried out at McGill University. The overall
132 objective was to evaluate and to improve, if needed, the current design practice for such
133 connections. Full-scale laboratory tests of extended shear tabs were first conducted [15-21]. These
134 tests assembled a database to better comprehend the nonlinear behaviour of shear tab connections.
135 The testing program was complemented with detailed finite element simulations. Several
136 parameters were interrogated to further our understanding regarding the behaviour of extended
137 shear tab beam to girder connections and improve their current design procedure. This paper
138 presents the findings from the corroborating finite element analysis of the research program.

## 139 2 Brief description of full-scale laboratory testing

140 Fifty-five full-scale laboratory tests were conducted at McGill University [15-21] to
141 characterize and further understand the behaviour of shear tab connections, including both standard
142 and extended configurations, beam-to-column and beam-to-girder arrangements, as well as bolted
143 and welded details. The connection configurations were designed in collaboration with practicing

structural engineers to reflect the current practice in North America. Among these tests, two specimens of full-depth extended beam-to-girder shear tabs with two vertical rows of three bolts (Figs. 4a and 4b) were selected to develop finite element models to further our understanding regarding their behaviour under gravity-induced shear forces; BG3-2-10-F [19] and BG3-2-13-F [20]. These specimens were nominally identical except for the thickness of the respective shear plate. In particular, the thickness of the shear plate of Specimen BG3-2-13-F was increased to satisfy the current compactness criteria for the stiffener of a plate girder as per CSA S16 [22] ( $200/\sqrt{F_y}$ ). This corresponds to the AISC 360 [2] width-to-thickness ratio for unstiffened elements subjected to axial compression (Table B4.1a, $0.45\sqrt{E/F_y}$ ). Of note, the shear plate compactness is not part of the AISC shear tab design method [1]; this method addresses unstiffened shear tab connections where plate local buckling is not a concern.

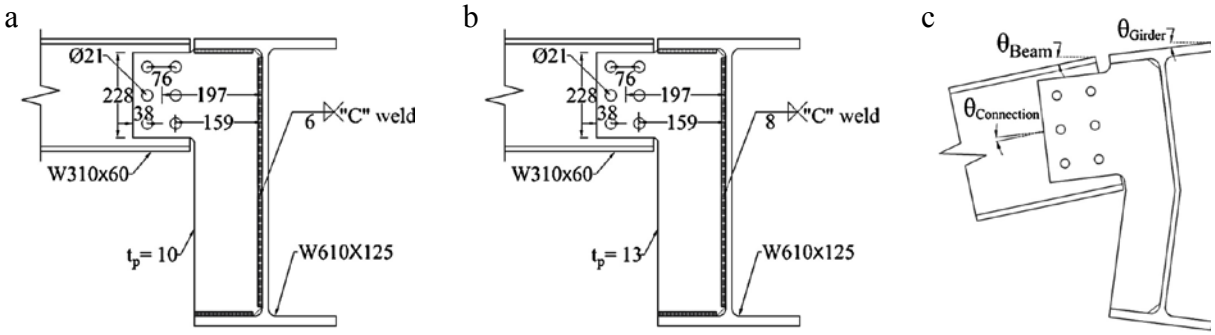


Fig. 4. Laboratory tests of beam-to-girder shear tabs: (a) details of Specimen BG3-2-10-F, (b) details of Specimen BG3-2-13-F, (c) measured rotations of specimens

The beam and girder were fabricated from ASTM A992 Grade 50 steel [23], while the shear plates were made of ASTM A572 Grade 50 steel [24]; for both grades the nominal $F_y$=345 MPa and $F_u$=448 MPa. To attach the shear tab to the supporting girder, an E71T (nominal $F_u$=490 MPa) electrode was used in a flux-cored arc welding process with additional shielding gas ($CO_2$) to provide a fillet weld on both sides of the plate. Each beam was snug tightened to the shear tab using 19 mm (3/4 in.) ASTM F3125 Grade A325 bolts [25] in standard size holes (20.6 mm (13/16

in.)). The test setup (Fig. 5a) consisted of a 12 MN and a 445 kN hydraulic actuator, a lateral bracing system for the steel beam, and supporting elements for the girder. The 12 MN actuator, located near the shear tab connection, developed the main shear force in the connection. The 445 kN actuator, placed at the far end of the beam, facilitated the vertical displacement control of the beam tip, as well as the connection rotation. Referring to Fig. 4c, the relative rotation between the beam and the girder was defined as the connection rotation. The lateral bracing system was installed to restrict the lateral displacement of the beam, without affecting its vertical displacement. This test setup, to apply simultaneous shear force and rotation to the connection, is based on that used in prior research [26].

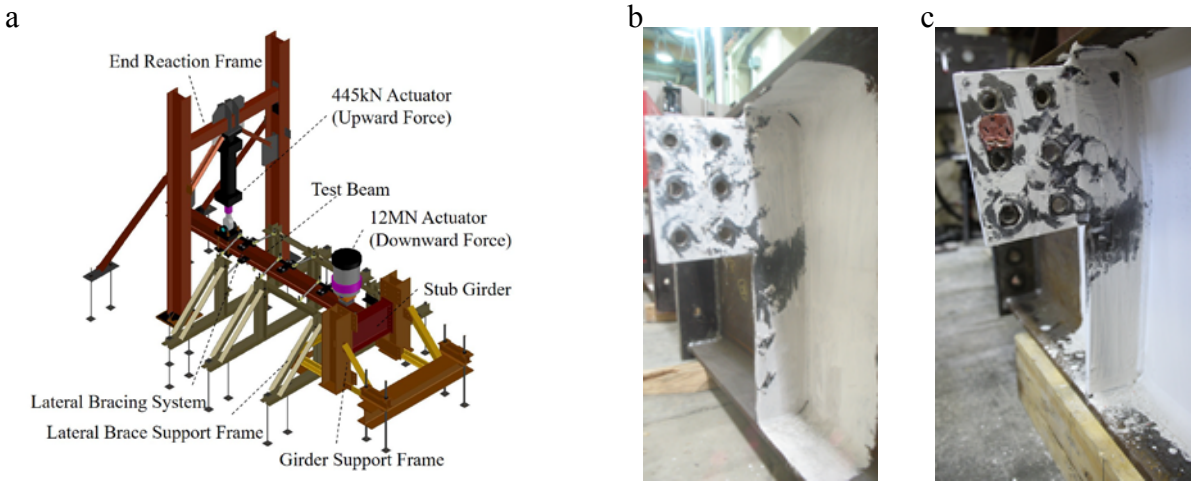


Fig. 5. Laboratory tests of beam-to-girder shear tabs: (a) test setup for, (b) deformed shape of specimen BG3-2-10-F, (c) deformed shape of specimen BG3-2-13-F

Referring to Fig. 6, Linear Variable Differential Transformers (LVDTs) were installed to measure the out-of-plane deformation of the beam, as well as that of the shear plate and of the girder web. In-plane rotation of the beam and girder were measured using inclinometers, as shown in Fig. 6. A complete description of the test programs can be found in [19, 20].

On the basis of the current AISC design procedure [1], Table 1 summarizes the calculated connection strengths corresponding to the probable failure modes. The contact between the shear plate and girder flanges was ignored; the shear plate was designed as would be done for an

unstiffened shear tab. Hence, the distance between the girder web and the interior bolt line (the *a* distance) was conservatively considered to be the unbraced length of the shear plate. Of note, this method resulted in a more conservative prediction for the shear plate buckling as compared to Fortney and Thornton's recommendation [14] for the connection eccentricity.

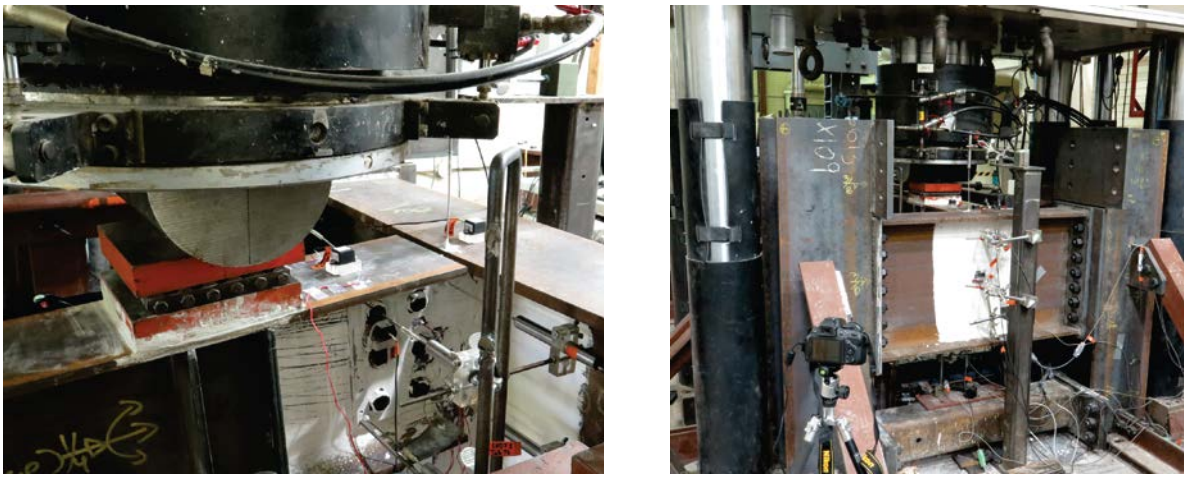

Fig. 6. Laboratory test of beam-to-girder shear tab specimen BG3-2-13-F

Table 1 AISC predicted strength of shear tab test specimens

| Failure mode | BG3-2-10-F | | | BG3-2-13-F | | |
|---|---|---|---|---|---|---|
| | Design strength (kN) | Expected strength[1] (kN) | Expected strength[2] (kN) | Design strength (kN) | Expected strength[1] (kN) | Expected strength[3] (kN) |
| Flexural and shear yielding of shear plate | 214 | 255 | 307 | 281 | 334 | 390 |
| Shear yielding of shear plate | 450 | 495 | 596 | 591 | 650 | 758 |
| Bolt bearing | 191 | 280 | 305 | 191 | 280 | 290 |
| Buckling of shear plate | 243 | 297 | 357 | 319 | 390 | 455 |
| Rupture at net section of shear plate | 318 | 509 | 496 | 417 | 667 | 654 |
| Bolt shear | 182 | 270 | 270 | 182 | 270 | 270 |
| Weld tearing | 1035 | 1380 | 1380 | 1294 | 1725 | 1725 |

[1]Expected strength based on probable material properties i.e.$R_yF_y$ (1.1 $F_y$) and $R_TF_u$ (1.2 $F_u$) for steel plates [27]
[2]Expected strength based on measured material properties i.e $F_y$=456MPa and $F_y$=525MPa for 10mm plate
[3]Expected strength based on measured material properties i.e $F_y$=442MPa and $F_y$=527MPa for 13mm plate

The buckling strength of the shear plate was calculated using two methods: rectangular plate buckling [1] and buckling of the double coped beam [4]. Both methods predicted that buckling would not prevent the shear plate to reach its fully plastic nominal flexural capacity ($M_p=F_yZ_p$). In addition to the nominal and expected material properties, the measured properties of the steel

beam, girder and plate were used to conduct these AISC-based calculations, whereas the nominal properties of the bolts and welds were relied on in this process.

Regarding the shear plate-to-girder weld, its size meets the AISC minimum requirement ( $a_w \geq 5/8t_p$ ), and the reported weld tearing strength is the concentric shear capacity of the vertical weld line. To ensure yielding of the shear plate in advance of bolt shear fracture, the AISC requirement for maximum shear plate thickness was controlled using the nominal yield stress of the shear plate, as well as its expected and measured material properties. Although both configurations meet this requirement, the bolt shear fracture was predicted as the governing failure mode in all cases, other than for calculations based on the expected material properties of Specimen BG3-2-10-F.

Contrary to the design predictions, bolt shear did not occur in any of the full-scale tests, nor did the bolts exhibit damage. The yielding and out-of-plane deformation of the girder web and the stiffened section of the shear tab (Fig. 5b and 5c), which was confined between the girder web and flanges, were observed as failure modes. The stiffness of specimen BG3-2-10-F degraded significantly at 221kN shear force (82% of the connection expected strength, i.e., 270kN) while specimen BG3-2-13-F lost its stiffness at 390kN shear force (144% of the connection expected strength, i.e., 270kN).

## 3 Finite element simulation of extended beam-to-girder shear tab connections

The finite element (FE) method was adopted to obtain a deeper understanding of the behaviour of extended beam-to-girder shear tab connections under gravity-induced shear forces. The main features of the developed FE models (Fig. 7) were chosen to be representative of those seen in the laboratory experiments; including geometry, boundary conditions, material properties, element size and element type, contacts and interactions, and the imposed loading protocol. The employed material properties were defined based on the engineering stress-strain curves obtained from

tensile coupon tests, directly extracted from the various components of the tested subassemblies. These were then converted to true stress-strain curves. The material properties for the bolt and welds were defined based on typical stress-strain curves, obtained from Kulak et al. [28] and Gomez et al. [29], respectively, which were scaled to meet the minimum specified values.

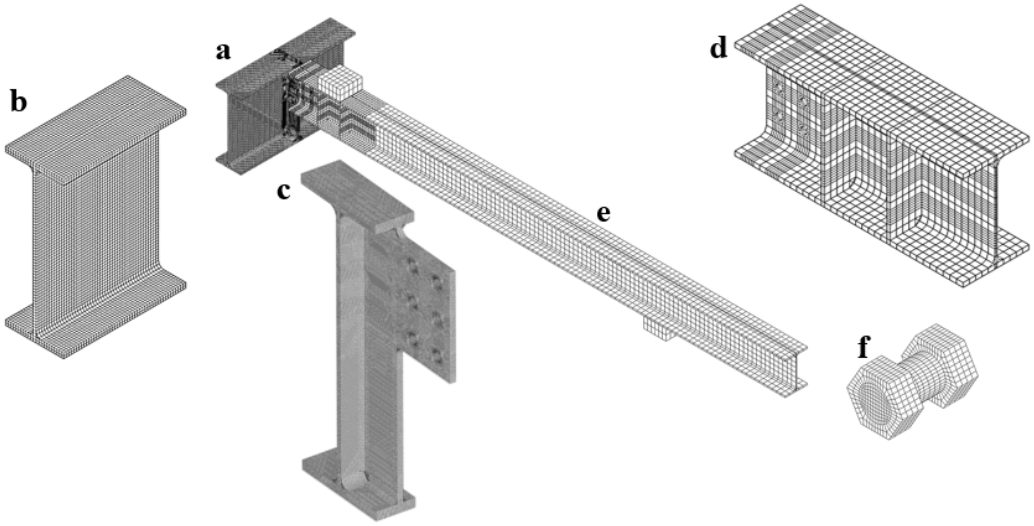


Fig. 7. Finite element model specifics: (a) overall model, (b) girder mesh (typical element size of 10 mm), (c) shear plate mesh (typical element size of 3 mm), (d) mesh of the beam in the vicinity of connection (typical element size of 20 mm), (e) beam mesh (typical element size of 40 mm), (f) bolt mesh (Typical element size of 1.5 mm)

First-order fully-integrated 3D solid elements were utilized to mesh the FE models of the shear tabs. Referring to Fig. 7, the element size was determined based on a mesh refinement analysis. To allow transmission of tangential force between components in contact, a friction coefficient of 0.3 was used for all surface-to-surface contact pairs, except those between the load cubes and the flanges of the beam where frictionless interaction was defined. Furthermore, to trigger possible local instabilities of the shear tab connection, local imperfections were introduced into the shear plate and girder. These local imperfections were proportioned to the limits of manufacturing tolerances for the web and flange of W-sections [30-32]. This approach was found to be satisfactory in prior FE studies associated with cross-section and member instabilities due to local and/or lateral torsional buckling (Elkady and Lignos [33]).

### 3.1 Comparison of numerical and experimental results

In order to evaluate the accuracy of the numerical models, their predictions were compared with the measured connection behaviour from the aforementioned laboratory tests. Among others, the developed shear force of the connection and the girder web out-of-plane deformation were chosen as the primary model verification criteria. The numerical model predictions are presented along with the experimental measurements in Fig. 8.

Referring to Figs. 8a to 8d, the predicted shear force response deviated from the test measurements only in the initial increments of the applied loading. This discrepancy is due to uncertainties related to the contact between the bolt shanks and the bolt holes for each specimen due to fabrication tolerances and installation of the respective test specimens. The shear tab connections were snug-tightened, hence, bearing between the bolt shanks and bolt holes transferred the shear force between the beam and the shear plate. Further, the initial position of each bolt in its hole was not controlled, leading to an unknown slip before contact bearing. In the FE model, the bolts were consistently placed at the centre of the bolt hole, resulting in an initial 0.8 mm (1/32 in.) gap around the entire perimeter of the bolt shanks, which matches the fabrication tolerance of standard 20.6mm (13/16in.) holes. To prevent rigid body motion of the beam, and consequently to overcome issues with numerical convergence of the FE model, a small amount of bolt pretension, i.e. 50 MPa, was applied. It has been shown that this level of pretension does not affect the global behaviour of similar numerical models [34].

Referring to Fig. 8f, the comparison between the girder web deformation of the numerical models and the test demonstrates that the FE models predict reasonably well the out-of-plane deformations of the girder web of Specimen BG3-2-13-F. For Specimen BG3-2-10-F (Fig. 8e), the girder web out-of-plane deformation was not accurately measured due to the malfunction of

LVDT6. In brief, the comparison of the FE simulation results with the experimental data suggest that the FE model is able to predict reasonably well the global and local response of extended beam-to-girder connections under gravity-induced loading.

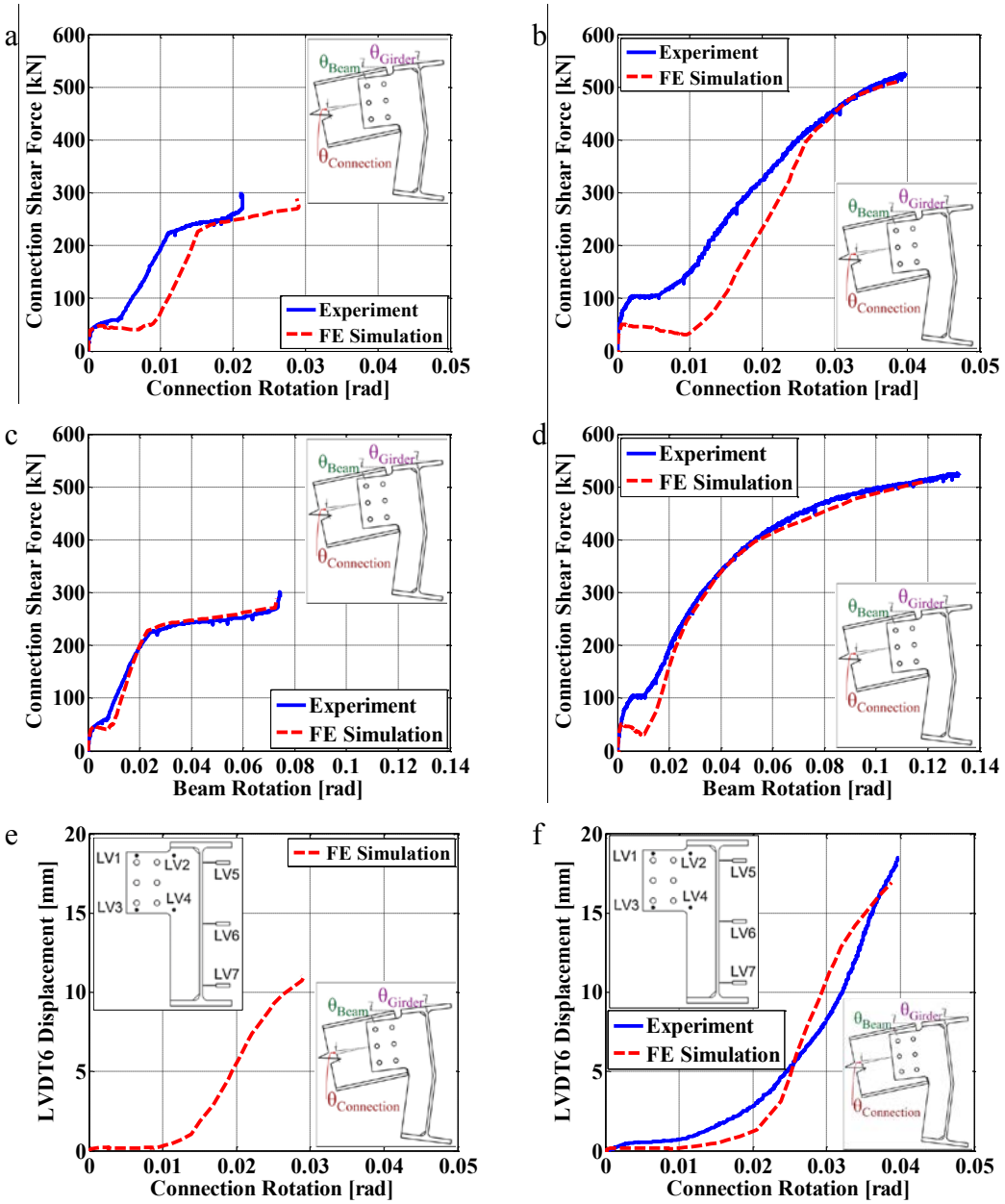


Fig. 8. Numerical model verification: (a) shear force versus connection rotation of specimen BG3-2-10-F, (b) shear force versus. connection rotation of specimen BG3-2-13-F, (c) shear force versus beam rotation of specimen BG3-2-10-F, (d) shear force versus beam rotation of specimen BG3-2-13-F, (e) girder web out-of-plane deformation versus connection rotation of specimen BG3-2-10-F, (f) girder web out-of-plane deformation versus connection rotation of specimen BG3-2-13-F

## 4 Parametric study for extended beam-to-girder shear tabs

The current AISC Steel Construction Manual [1] provides design equations to account for the various failure modes that may occur in a shear tab connection. It is rather challenging and costly to evaluate the accuracy of an individual design equation by solely conducting physical experiments on shear tabs. One reason is the interaction of the different failure modes after the specimen exhibits inelastic behaviour. The FE model allows for the systematic evaluation of each failure mode of interest separately, including the applicability of the current design equations. As such, a parametric study was conducted in which the strength of the connection components (beam, shear plate, bolts, and girder) were determined. In this process, the calibrated FE models for specimens BG3-2-10-F and BG3-2-13-F served as baseline models.

Table 2-Features and capabilities of FE models

| Model Notation | Features | Aspect Determined |
|---|---|---|
| FE-E | All components elastic | Elastic stiffness and elastic buckling strength |
| FE-E-G | All components elastic except girder | Out-of-plane bending capacity of girder web |
| FE-E-Be | All components elastic except beam | Effect of beam yielding on response of connection |
| FE-E-Bo | All components elastic except bolts | Shear capacity of bolt group |
| FE-E-SH | All components elastic except shear plate | Strength of shear plate |
| FE-Pl | Yieldable material properties assigned to all components | Strength of connection and interactions between failure modes |
| FE-Pl-Imp | Yieldable material properties assigned to all components. Initial imperfections assigned to trigger buckling of shear tab | Effect of initial imperfection on behaviour of shear tab |

The individual FE model features and findings are presented in Table 2 and are further discussed in Sections 4.1 and 4.2. Referring to Table 2, in the FE-E model it was assumed that all the material properties were elastic such that the elastic stiffness of the shear tab connection could be computed. The inelastic material properties for each component were then included in the FE model following a step-by-step process. The FE-E model was used to determine the load transfer mechanism of the connection, while the results of the FE models with damageable components gave an opportunity to

comprehend the load redistribution due to material nonlinearity and/or geometric instabilities occurring within a connection. Both single- and double-sided shear tabs were investigated.

### 4.1 Single-sided shear tabs

The results of the parametric study for Specimens BG3-2-10-F and BG3-2-13-F are illustrated in Figs. 9 and 10, respectively. The shear force of Specimen BG3-2-10-F is presented versus the connection rotation and the beam rotation in Figs. 9a and 9b, respectively. Displacements of LVDT 4 and LVDT 6 (Figs. 8e and 8f) are presented versus the connection rotation in Figs. 9c and 9d, respectively.

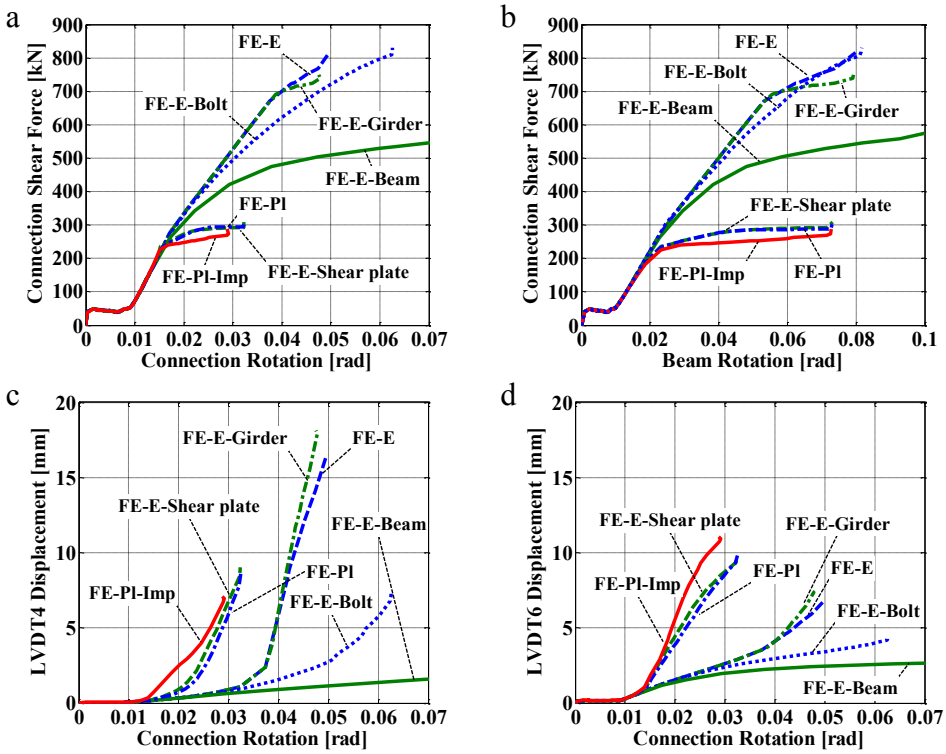


Fig. 9. Predictions of numerical models for specimen BG3-2-10-F: (a) shear force versus connection rotation, (b) shear force versus beam rotation, (c) out-of-plane deformation of shear plate versus connection rotation, (d) out-of-plane deformation of girder web versus connection rotation

Referring to Figs. 9 and 10, the FE model with elastic properties (FE-E) suggests a practically bilinear response. These FE models significantly lost their stiffness when the slope of the out-of-

plane deformation of the shear plate (LVDT4) increased. This stiffness change is associated with the bifurcation point due to elastic buckling. Figures 9d and 10d show a significant increase in the girder web out-of-plane deformation slope (LVDT6) following the shear plate elastic buckling. A comparison between the elastic model (FE-E) and the model with a yieldable girder (FE-E-G), demonstrated that their response was approximately identical prior to the onset of girder web yielding. For the slender shear tab (Specimen BG3-2-10-F), Fig. 9a shows that the connection with a yieldable girder lost its stiffness and reached its capping strength soon after the shear plate buckled. The strength plateau of the FE-E-G model was attributed to yielding of a large part of the girder web, due to the out-of-plane bending, and the formation of what has been denoted as the

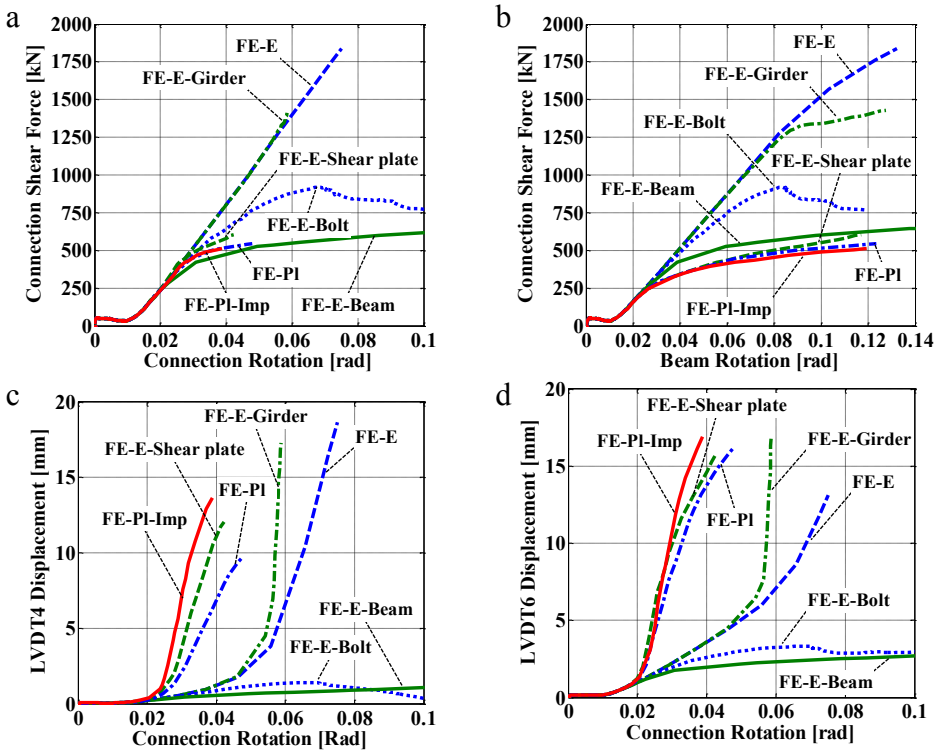


Fig. 10. Predictions of numerical models for specimen BG3-2-13-F: (a) shear force versus connection rotation, (b) shear force versus beam rotation, (c) out-of-plane deformation of shear plate versus connection rotation, (d) out-of-plane deformation of girder web versus connection rotation

"girder mechanism". In contrast, Fig. 10a shows that the FE-E-G model of the compact shear tab (Specimen BG3-2-13-F) lost its stiffness prior to the shear plate elastic buckling due to the shear yielding of the bottom part of the girder web.

Figures 9 and 10 demonstrate the great dependency of the connection response on the yielding of the shear plate. The yieldable shear plate, i.e. shear plate of models FE-E-SH, FE-Pl, and FE-Pl-Imp, began to yield at the lower re-entrant corner (Figs. 11a and 11b) while its out-of-plane deformation was negligible. As the shear force increased, the yielding propagated to the stiffened part of the shear plate and its out-of-plane deformation increased. Referring to Fig. 9a, the slender shear plate (BG3-2-10-F) lost its stiffness when yielding propagated through the full width of its stiffened portion (Figs. 11c and 11d). In contrast, Fig. 10a shows that the compact shear tab (Specimen BG3-2-13-F) was able to continue resisting shear after yielding of the stiffener, although its stiffness slightly decreased at this point.

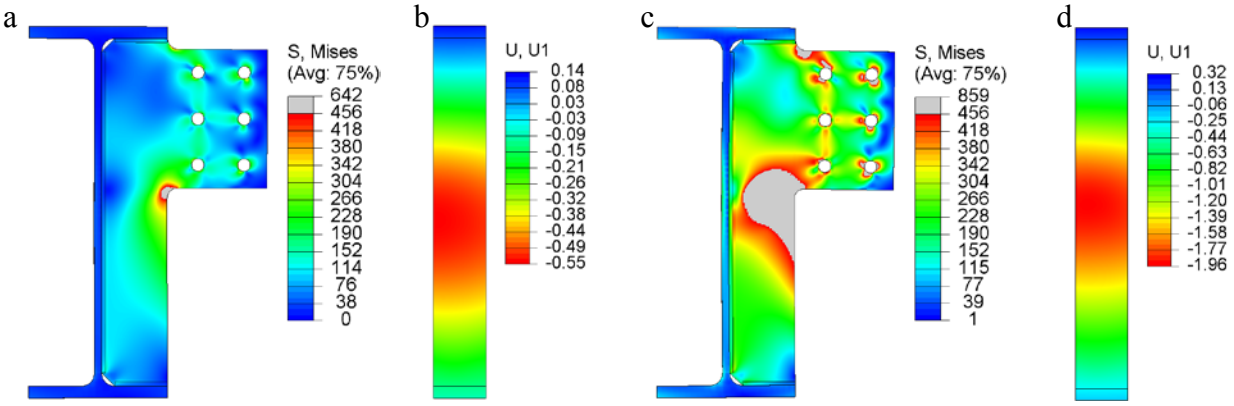


Fig. 11. Prediction of model FE-E-SH of specimen BG3-2-10-F for: (a) stress of shear plate at θ=0.0115 rad, (b) out-of-plane deformation of girder web at θ= 0.0115 rad, (c) stress of shear plate at θ= 0.0155 rad, (d) out-of-plane deformation of girder web at θ= 0.0155 rad (The grey colour represents yielded regions)

In comparison to FE-E-SH model, the girder web of the FE-Pl model began to yield soon after yielding of the stiffener, which resulted in a slightly lower shear force at the end of the analysis. Referring to Figs. 9 and 10, the shear plate and the girder web of the model incorporating imperfections experienced a larger out-of-plane deformation at the same level of shear force as compared with model FE-Pl. In comparison to model FE-Pl, this imperfection resulted in a slight decrease in the capping strength (9% and 5% for Specimens BG3-2-10-F and BG3-2-13-F, respectively) of the model FE-Pl-Imp.

## 4.2 Double-sided shear tabs

As presented in the Section 4.1, the girder web out-of-plane deformation influenced the failure mode of single-sided shear tabs. However, the contribution of this failure mode may be insignificant for double-sided shear tab connections, where two beams, one framed to each side of the girder, counterbalance the moments of each other. To investigate the behaviour of double-sided shear tabs, a series of finite element analyses were conducted for specimens BG3-2-10-F and BG3-2-13-F. To decrease computational costs, symmetric boundary conditions were implemented along the girder axis; a beam and half of girder section were included in these FE models. The results of the parametric study for Specimens BG3-2-10-F and BG3-2-13-F are presented in Fig. 12.

Referring to Figs. 12a and 12b, the bifurcation point due to elastic buckling of the shear plate was observed in the slender shear tab (Specimen BG3-2-10-F) while the stiffness of the connection with a compact shear plate (Specimen BG3-2-13-F) remained constant, even though its shear plate experienced large out-of-plane deformations. The FE model response with a yieldable girder was identical to the elastic model up to the yielding of the girder web. As the out-of-plane deformation of the girder web was restricted, the girder web yielded due to the applied shear force. This girder web yielding mechanism is in contrast to the yielding mechanism of the single-sided configuration in which the girder web yielding began mainly due to its out-of-plane bending. For the numerical model containing a yieldable shear plate, the onset of yielding occurred at the both re-entrant corner of the shear plate when its out-of-plane deformation was negligible. Unlike the single-sided connections, the yielding propagated along the bolt line instead of the stiffened part of the shear plate. The total height of the shear plate along the bolt line, closest to the girder, yielded and the connection stiffness decreased significantly at this point.

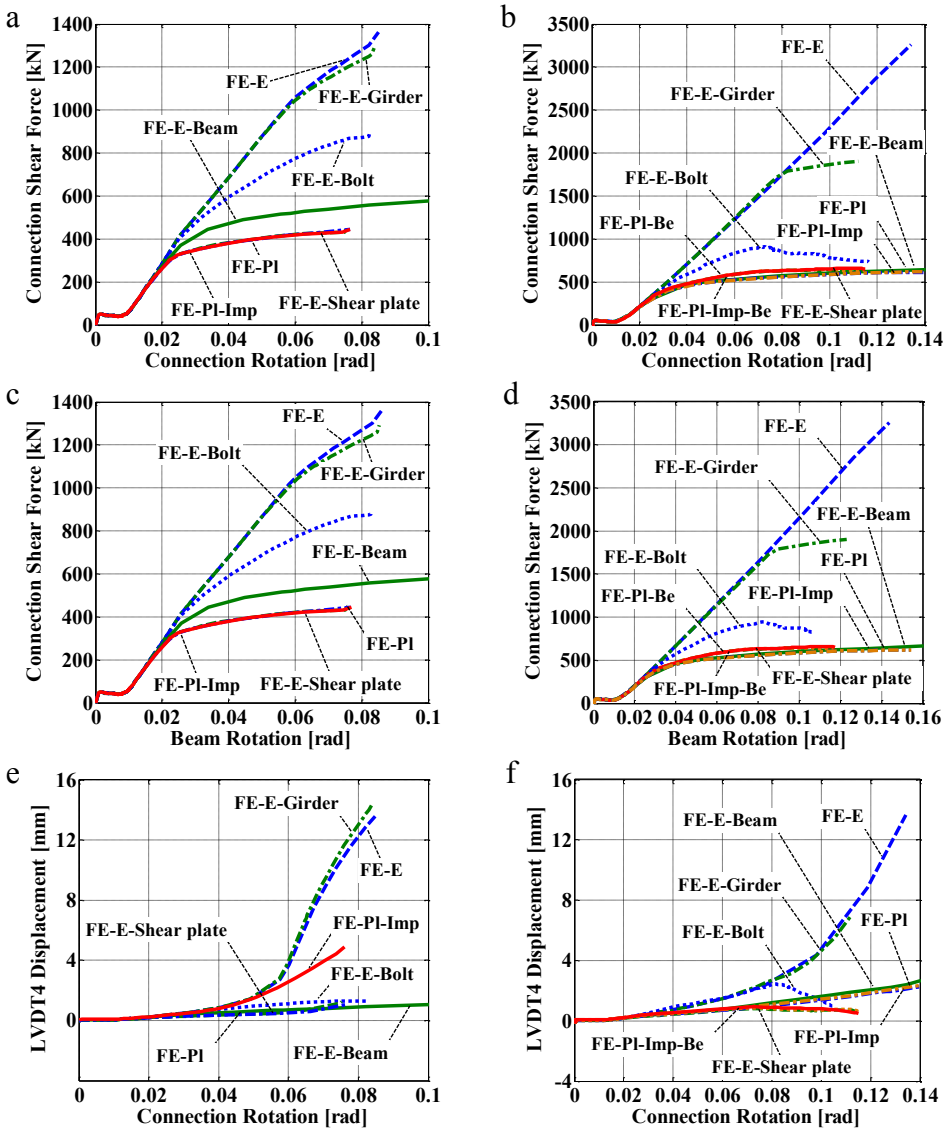


Fig. 12. FE models for double-sided shear tabs: (a) prediction for shear force versus connection rotation of specimens BG3-2-10-F, (b) prediction for shear force versus connection rotation of specimens BG3-2-13-F, (c) prediction for shear force versus beam rotation of specimens BG3-2-10-F, (d) prediction for shear force versus beam rotation of specimens BG3-2-13-F, (e) prediction for out-of -plane deformation of shear plate versus connection rotation of specimens BG3-2-10-F, (f) prediction for out-of -plane deformation of shear plate versus connection rotation of specimens BG3-2-13-F

Figure 12 shows that the predictions of the FE-Pl and FE-Pl-Imp models of Specimen BG3-2-10-F were close to those of the model with a yieldable shear plate. This occurred because the corresponding shear force demand was not sufficient to develop yielding in the girder web, as shown in Fig. 12. However, after yielding of the full depth of the shear plate along the interior bolt line of model FE-Pl-Imp (Fig. 13a), yielding propagated at the stiffened portion of the shear plate

(Fig. 13c) and its out-of-plane deformation increased. Referring to Fig. 12b, the results of models FE-Pl and FE-Pl-Imp of Specimen BG3-2-13-F deviated from the results of the model FE-E-SH due to the beam web yielding along the net section of vertical row of bolts, farthest from the girder. As the main purpose of this study was to investigate the behaviour of the shear tab connection, the effect of beam yielding was prevented from dominating the results of the numerical model FE-Pl-Be by assigning elastic material properties to the beam while the other components were defined to experience yielding. Figure 12b shows that the results of this model and model FE-Pl-Imp-Be, were identical to the model with a yieldable shear tab because the level of shear force was not sufficient to initiate yielding of the girder web.

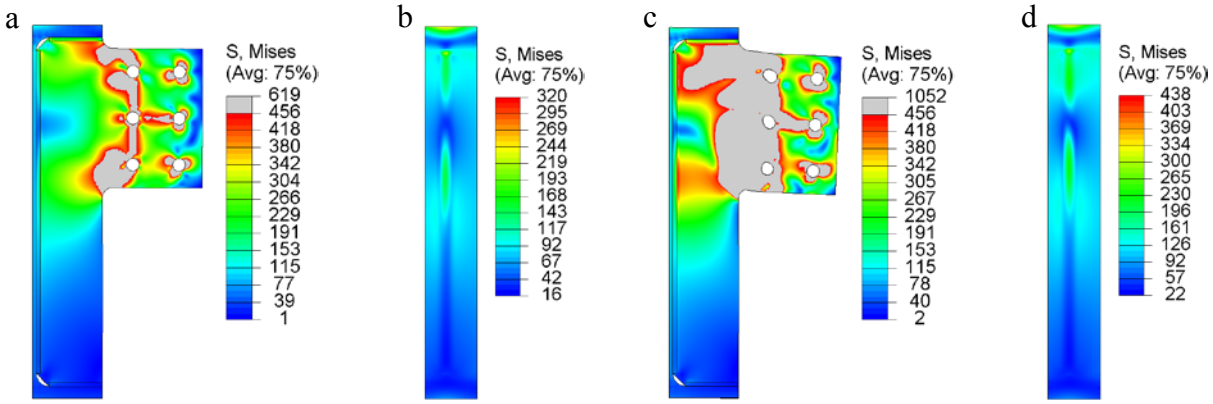


Fig. 13. Prediction of model FE-Pl-Imp of specimen BG3-2-10-F for stress of: (a) shear plate at θ=0.0223 rad, (b) girder web at θ=0.0223 rad, (c) shear plate at θ=0.0603 rad, (d) girder web at θ=0.0603 rad (The grey colour represents yielded regions)

## 5 Discussion

A comparison of the results of the laboratory tests and numerical models for single-sided shear tabs with the results of the FE models of double-sided shear tabs demonstrated that the expected failure mode is different for the two configurations. Figure 14a shows a free body cut for selected sections of the shear plate. This method of evaluation was employed to examine the different load transfer mechanisms in single and double-sided shear tabs. Using these free body cuts, the location of the inflection point was determined (Fig. 14b) and its distance to the centreline of the girder

web, i.e. the effective eccentricity ($e_{eff}$), and the centroid of the bolt group, i.e. the bolt group eccentricity ($e_b$), were calculated. The results of free body cuts are presented and discussed in Sections 5.1 and 5.2.

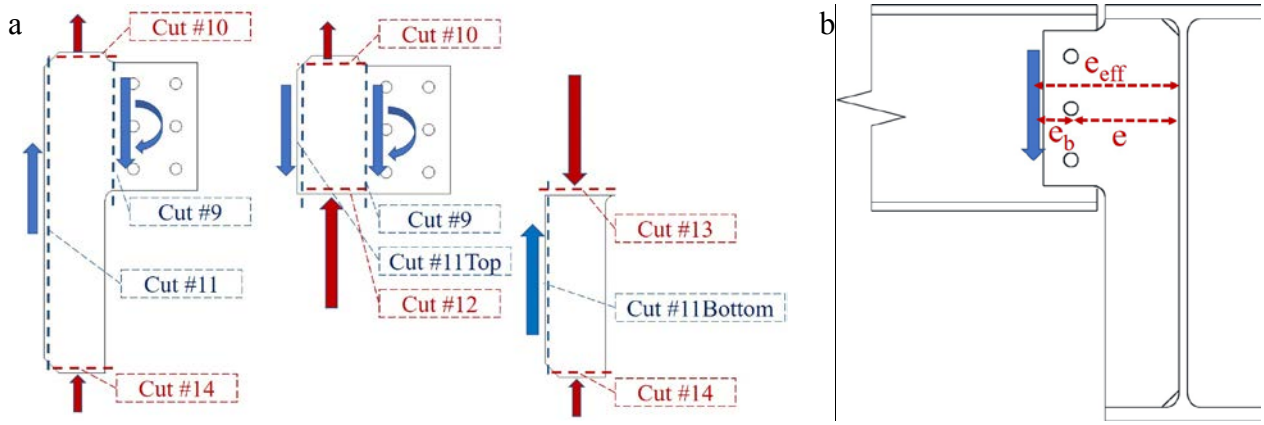


Fig. 14: (a) defined sections for Free body cuts, (b) connection eccentricity

## 5.1 Load transfer mechanism

As shown in Figs. 15a and 15c, the compressive axial force, which developed in the stiffened portion of the shear tab (Cut #12), was larger than the connection shear force of the single-sided shear tabs. In contrast, this compressive axial force was smaller than the connection shear force in the double-sided shear tabs (Figs. 15b and 15d). For elastic models (FE-E) of Specimens BG3-2-10-F and BG3-2-13-F, the ratio between the stiffener axial force and the connection shear force was 1.67 and 0.48 for single-sided and double-sided shear tabs, respectively. As these ratios remained constant for both the slender and compact shear tabs, it can be concluded that they result from the different loading transfer mechanisms for single and double-sided shear tabs.

In order to determine the load transfer mechanism, the forces, developed through different portions of the shear plate, were also studied. Regarding the elastic models of Specimen BG3-2-10-F (including single-sided and double-sided), the vertical forces at the shear plate are presented versus the beam rotation in Fig. 16. A large component of the connection shear force of single-sided

shear tabs (i.e. Cut #9) was transferred to the girder web (i.e. Cut #11) as a shear force, while the girder flanges (Cut #10 and Cut #14) tolerated 20% of the connection shear.

Notably, the shear force was not distributed uniformly over the girder web depth, which contradicts the assumptions made in the design procedure of the shear tab connection. Referring to Fig. 16c, the shear force at the top part of the stiffener (Cut #11Top) developed in the downward direction to counterbalance the moment, mobilized due to the existing eccentricity of the external shear force.

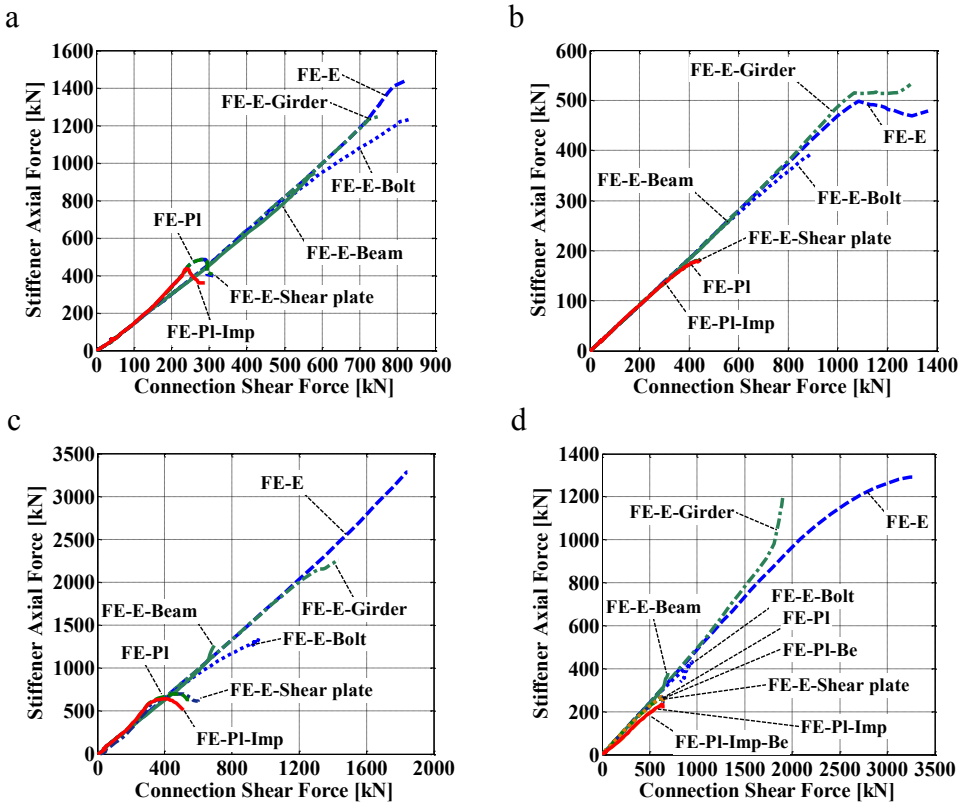


Fig. 15. Predictions of the developed axial force at the stiffener versus the connection shear force for: (a) single-sided configuration of specimen BG3-2-10-F, (b) double-sided configuration of specimen BG3-2-10-F, (c) single-sided configuration of specimen BG3-2-13-F, (d) double-sided configuration of specimen BG3-2-13-F

Further, horizontal forces developed at the stiffener, along the edges of the extended portion of the shear plate, to counterbalance the bending moment applied to the shear plate at Cut #9. Referring to Fig. 16c, the slope of the curve representing the axial force of the stiffener decreased significantly at 1129 kN compression, which corresponds to a connection shear force equal to 672 kN (0.0375

rad). Referring to Fig. 16d, unlike the single-sided shear tabs, the shear force that was developed at the top portion of the stiffener (Cut #11Top) of the double-sided shear tabs was an upwards force that counterbalanced a significant portion of the connection shear force; therefore, the stiffener was subjected to a lower compression force although the double-sided connection was subjected to a

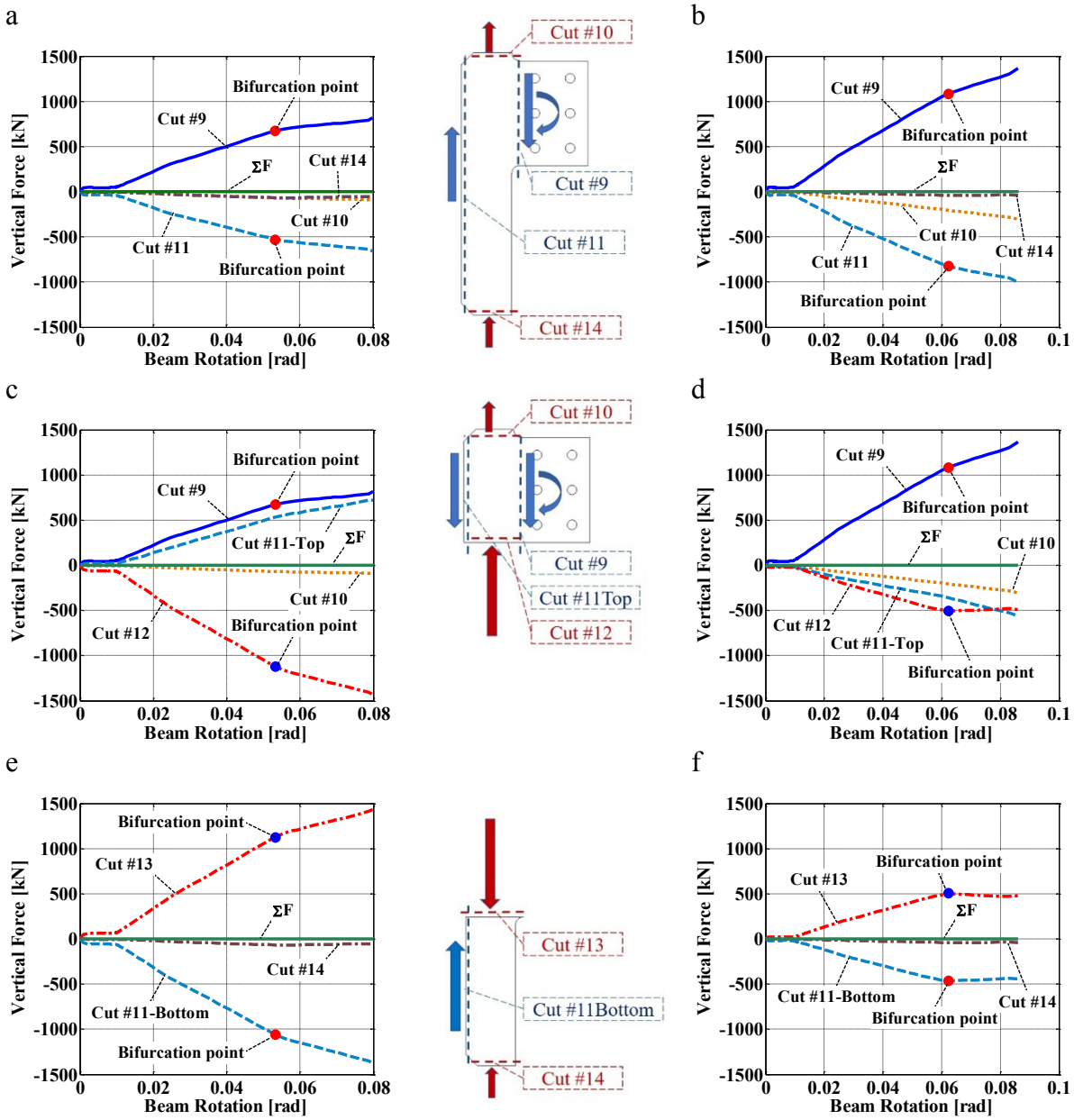


Fig. 16. Prediction of elastic FE models of specimen BG3-2-10-F for vertical force at: (a) stiffener of single-sided connection, b) stiffener of double-sided connection, (c) top part of the stiffener of single-sided connection, (d) top part of the stiffener of double-sided connection, (e) bottom portion of the stiffener of single-sided connection, (f) bottom portion of the stiffener of double-sided connection

higher level of applied shear force in comparison to the single-sided shear tab. The shear tab buckled at 508 kN compression force, which is half the buckling force observed in the single-sided shear tab.

This observation can be attributed to the fact that the stiffener was subjected to the larger horizontal shear stress along the bottom re-entrant corner. The horizontal shear stress was mobilized in the stiffener because of the bending moment that developed in the shear tab connection. Due to the higher stiffness of the double-sided shear tab, its inflection point formed farther from the girder as compared to the single-sided shear tab. The upward shear force along Cut #11-Top and applied shear force along the Cut#9 formed a shear force couple, which applied an extra moment on the stiffener that was counterbalanced by the horizontal force developed in the stiffener. Therefore, the stiffener of the double-sided shear tab was subjected to a much higher horizontal shear stress as compared to the single-sided shear tab. The top flange of the girder resisted 20% of the connection shear force while the bottom flange negligibly contributed to transfer the connection shear force.

Note that the shear plate yielding affected the load transfer mechanism. In single-sided shear tabs, the stiffened portion of the shear plate yielded in advance of its elastic buckling. This local yielding resulted in the application of a transverse force to the girder web, which was resisted by out-of-plane bending. Yielding then occurred due to the limited out-of-plane bending capacity of the girder web, which resulted in the formation of the girder web mechanism. Comparisons between the results of single-sided connections illustrated the shear plate's susceptibility to inelastic buckling when the compactness limit for stiffeners was not met. The slender stiffener (Specimen BG3-2-10-F) became unstable and reached its strength plateau as soon as it yielded locally, while the compact stiffener (Specimen BG3-2-13-F) reached a higher shear force after the local yielding of the shear plate, which is a stable failure mechanism.

447 The yielding of the shear plate along the net section of the vertical row of bolts, closest to the
448 girder, was observed as the governing failure mode for double-sided shear tabs. The observed
449 strength of double-sided shear tabs for Specimens BG3-2-10-F and BG3-2-13-F (430 kN and 630
450 kN, respectively) was close to the predictions for the rupture of their shear plate at the net section
451 (496 kN and 654 kN for BG3-2-10-F and BG3-2-13-F, respectively). Notably, after yielding along
452 the bolt line, yielding propagated to the stiffener of Specimen BG3-2-10-F and its out-of-plane
453 deformation started to increase. This observation demonstrates that inelastic buckling of the
454 stiffener may also occur in double-sided configurations; which prevents the connection from
455 reaching the shear force corresponding to rupture along the net section.

456 **5.2 Effective eccentricity**

457 Based on the shear force and bending moment developed in the shear plate and the bolt group,
458 the location of the inflection point was determined. Figure 17 illustrates the distance between the
459 inflection point and the centroid of the girder web, i.e. the effective eccentricity ($e_{eff}$ in Fig. 14b),
460 for the various connection configurations. In contrast to the current design assumption, the
461 inflection point forms away from the girder web, farther than the centre of the bolt group (Fig. 17);
462 which means $e \leq e_{eff}$. As shown, the shear plate buckling, yielding of the shear plate, yielding of
463 bolts, and the girder web yielding decreased the connection's stiffness and pushed the inflection
464 point toward the girder. The only exception to this observed trend is the FE-E-G model of the
465 double-sided configuration of Specimen BG3-2-13-F, for which the shear force reached the
466 girder's shear yielding capacity. Comparisons between the single and double-sided configurations
467 of Specimens BG3-2-10-F (Fig. 17a and 17b) and BG3-2-13-F (Fig. 17c and 17d) demonstrated
468 the larger eccentricity of the double-sided configuration at the same level of shear force. This
469 observation can be attributed to the higher stiffness of the double-sided configuration in

comparison with the single-sided one. Moreover, the implementation of a thicker plate for the shear tab of Specimen BG3-2-13-F resulted in a higher stiffness and a larger eccentricity under the same level of shear force.

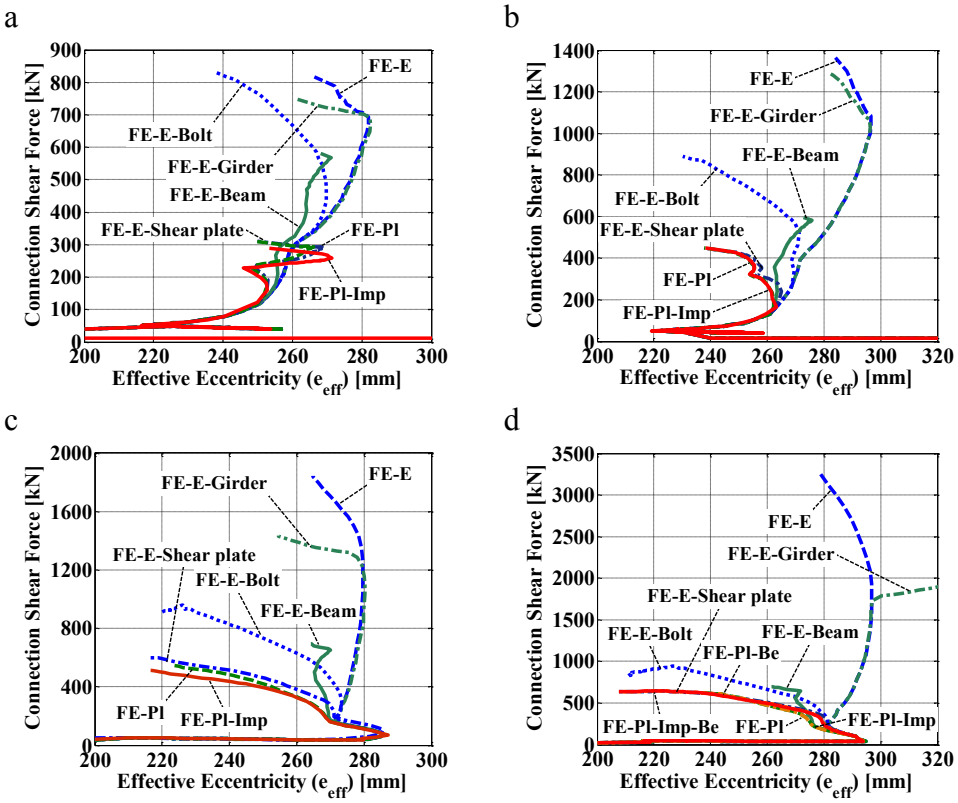


Fig. 17. Predictions of numerical models for shear force versus effective eccentricity at: (a) single-sided configuration of Specimen BG3-2-10-F, (b) double-sided configuration of Specimen BG3-2-10-F, (c) single-sided configuration of Specimen BG3-2-13-F, (d) Double-sided configuration of Specimen BG3-2-13-F

The comparison between predictions of the model with a yieldable bolt group (FE-E-Bo) and the model with the yieldable components (FE-Pl) demonstrated that the shear strength of the bolt group was much higher than the shear capacity of the connection. The ratio between the bolt shear strength and the shear capacity of the connection was between 3.0 (single-sided configuration of specimen BG3-2-10-F) and 1.4 (double-sided configuration of Specimen BG3-2-13-F). The FE model prediction was compared with available bolt shear experiments [35, 36] in order to ensure the capability of the FE model to detect accurately the bolt shear strength. Furthermore, the deformation of an individual bolt was compared with 8.64 mm (0.34 in.) as the fracture criterion

484 to determine the bolt shear strength of the models with yieldable bolts (FE-E-Bo). The AISC
485 Manual [1] implemented this limit as the fracture criterion in its instantaneous centre of rotation
486 (ICR) method to calculate the shear strength limit corresponding to the shear fracture of the bolt
487 group.

488 Furthermore, as shown in Table 3, the observed bolt shear strength of models FE-E-Bo was
489 much higher than the AISC predictions based on the ICR method. This over-strength can be
490 attributed to the eccentricity of the bolt group ($e_b$ distance in Fig. 14b) being much smaller than
491 the AISC recommendation for eccentricity ($e$ distance in Fig 14b). Based on these observations, it
492 would be reasonable to determine the bolt shear strength of the connection based on the bolt group
493 eccentricity ($e_b$) that is equal to the distance between the location of inflection point and the centre
494 of the bolt group. Notably, the observed bolt group eccentricity should not be extended to
495 configuration with different bolt pattern as previous research [36] has demonstrated the connection
496 eccentricity as a function of the bolt pattern depth. Further studies are needed to propose an
497 equation for the bolt group eccentricity.

498 Table 3-Bolt shear strength based on predictions of the model FE-E-Bo

| Specimen | FE Model | | AISC Design Method | | | New Recommendations | | |
|---|---|---|---|---|---|---|---|---|
| | Inflection point [a] (mm) | $V_u$ Shear Strength (kN) | Eccentricity (mm) | $V_{SH}$ Shear Strength (kN) | $\frac{V_u}{V_{SH}}$ | Bolt Group Eccentricity (mm) | $V_{SH}$ Shear Strength (kN) | $\frac{V_u}{V_{SH}}$ |
| BG3-2-10-F–S.S [b] | 230 | 879 | 197 | 270 | 3.26 | 27 | 786 | 1.12 |
| BG3-2-10-F–D.S [c] | 236 | 871 | 197 | 270 | 3.23 | 33 | 754 | 1.16 |
| BG3-2-13-F–S.S [b] | 229 | 918 | 197 | 270 | 3.40 | 27 | 786 | 1.17 |
| BG3-2-13-F–D.S [c] | 233 | 896 | 197 | 270 | 3.32 | 30 | 771 | 1.16 |

499 a) Distance between the location of inflection point and the centre of girder web
500 b) Suffix S.S refers to single-sided configuration
501 c) Suffix D.S refers to double-sided configuration

502 As shown in Table 3, this revised definition of the bolt group eccentricity resulted in a
503 reasonably conservative prediction of the bolt shear strength of the connection (The ratio between
504 FE result and prediction based on new recommendation was between 1.12 and 1.16). Notably, the

505 model FE-E-Bo of the single-sided configuration of Specimen BG3-2-10-F did not experience bolt
506 fracture when it was subjected to the displacement loading protocol corresponding to the
507 laboratory test. Therefore, the model was subjected to the adjusted loading protocol to obtain a
508 resistance for the bolt shear fracture failure mode. The smaller ratio between the FE and analytical
509 predictions in Specimen BG3-2-10-F, were attributed to the slender shear tab experiencing a larger
510 out-of-plane deformation as compared to the compact shear tab. Therefore, the two bottom bolts
511 were subjected to a larger axial deformation from the out-of-plane movement of the shear tab.

512 Furthermore, the experimentally measured strength of the single-sided specimen BG3-2-13-F
513 (520 kN) was much larger than the design strength, which was based on the shear failure of the
514 bolt group calculated using the instantaneous centre of rotation analysis method with the
515 eccentricity equal to the distance between the centre of the bolt group and the weld line (270 kN),
516 i.e. as per the current practicing design method. This observation further validated the prediction
517 of the FE models with respect to the formation of the inflection point along the exterior bolt line.

518 **6 Conclusions**

519 Owing to the lack of a comprehensive published procedure for the design of stiffened extended
520 shear tab connections, practicing engineers often use the current AISC design procedure, even
521 though it was originally developed for unstiffened extended shear tabs. This method assumes that
522 the inflection point forms at the face of the supporting girder or column and that the weld
523 attachment between the shear plate and the girder flanges (i.e., stabilizer plates) is ignored.
524 Experiments on stiffened extended shear tabs have demonstrated that these weld attachments
525 influence the load transfer mechanism within the connection. Therefore, there is concern with
526 respect to the validity of the aforementioned design assumptions.

To evaluate and improve the current design practice for extended shear tabs, full-scale laboratory tests and complementary finite element simulations were conducted. This paper contains a summary of the finite element studies. The numerical models were validated with previously conducted full-scale experiments on representative beam-to-girder connections. The main findings of the corroborating FE study are summarized as follows:

- The inflection point of extended beam-to-girder shear tabs with full depth shear plates is away from the girder centreline (i.e. farther from the centre of the bolt group) in both the single- and double-sided configurations. Hence, the current practice for design of these connections may not be always conservative as it underestimates the force demands on the stiffened portion of the shear tab.
- The stiffened portion of extended beam-to-girder shear tabs with full-depth shear plates (including single-sided and double-sided configurations) is subjected to vertical axial and horizontal shear forces simultaneously. This is not considered in the current design procedure. The axial and shear force demands are strongly dependent on the out-of-plane stiffness of the girder web and the connection eccentricity.
- Single-sided extended beam-to-girder shear tabs with full-depth shear plate experience yielding in their stiffened portion along the bottom re-entrant corner. Out-of-plane deformations tend to increase in such case.
- Single-sided extended beam-to-girder shear tabs with full-depth shear plates experience shear forces much higher than those anticipated based on design values representative of shear failure of the bolt group. This demonstrates that the bolt group eccentricity is significantly smaller than the assumed value, the distance between the weld line and the centre of the bolt group.

- The ultimate shear capacity of the bolt group can be determined by calculation on the basis of the bolt group eccentricity, the distance between the inflection point and the centre of the bolt group. For the studied bolt pattern (i.e., two vertical lines of three bolts), the inflection point shall be considered conservatively at the vertical line of bolts, farthest from the girder. Of note, this location is not representative of connections with different bolt pattern because the location of the inflection points is a function of the bolt pattern depth. Additional studies are necessary to develop an empirical equation for the bolt group eccentricity.
- In the absence of a robust method to predict the buckling strength of the stiffened portion of the shear plate, the local buckling failure mode of the shear plate should be considered. The use of shear plates that satisfy the CSA S16 compactness ratio for stiffeners ( $200/\sqrt{F_y}$ ) results in a stable shear tab connection behaviour.
- The behaviour of double-sided extended beam-to-girder shear tabs with full-depth shear plates differs from that of single-sided connections. In comparison to the single-sided connections, a much lower compressive force develops in the stiffener of a double-sided connection while the connection is subjected to a higher shear force. In advance of yielding of the stiffened portion of the shear plate, these connections experience shear plate yielding at the net section of the vertical row of bolts, closest to the girder.

## 7 Acknowledgments

The authors would like to thank the ADF Group Inc. and DPHV Structural Consultants for their generous technical and financial support, as well as the Natural Sciences and Engineering Research Council of Canada. The authors also thank Jacob Hertz and Nathan Goldstein Apt for sharing their experimental results for extended shear tabs. The finite element computations were conducted on the

McGill University supercomputer Guillimin, which is managed by Calcul Québec and Compute Canada. The supercomputer operation is funded by the Canada Foundation for Innovation (CFI), NanoQuébec, RMGA and the Fonds de recherche du Québec - Nature et technologies (FRQ-NT).

## 8 References

[1] AISC 325-17, Steel Construction Manual, 15th edition, American Institute of steel Construction, Chicago, IL, 2017. (Chapter 7: pp.6-8, Chapter 9: pp.6-10, Chapter 10: pp.87-91 & 127-132)

[2] AISC 360-16, Specification for Structural Steel Buildings, American Institute of Steel Construction, Chicago, IL, 2016.

[3] B. Dowswell, R. Whyte, Local stability of double-coped beams, Eng. J. AISC, 51(1) (2014), pp. 43–51.

[4] AISC 325-11, Steel Construction Manual, 14th edition, American Institute of steel Construction, Chicago, IL, 2011. (Chapter 9: pp.6-10)

[5] J.J. Cheng, J.A. Yura, C.F. Johnson, Design and behavior of coped beams, University of Texas at Austin, Austin, TX, 1984.

[6] L.S. Muir, W.A. Thornton, Survey of Existing Studies on Strength and Deformation of Spherical Joints in Steel Space Trusses, Eng. J. AISC, 41 (3) (2004), pp. 133–134.

[7] L.S. Muir, C.M. Hewitt, Design of unstiffened extended single-plate shear connections, Eng. J. AISC, 46 (2) (2009), pp. 67-79.

[8].W.A. Thornton, P.J. Fortney, On the need for stiffeners for and the effect of lap eccentricity on extended single-plate connections, Eng. J. AISC, 48(2) (2011),pp. 117-125.

[9] A. Elkady, D.G. Lignos, Full-scale testing of deep wide-flange steel columns under multiaxis cyclic loading: loading sequence, boundary effects, and lateral stability bracing force demands, J. Struct. Eng. ASCE, 144 (2) (2018), 04017189.

[10] D.R. Sherman, A. Ghorbanpoor, Design of extended shear tabs, University of Wisconsin-Milwaukee, Milwaukee, WI, 2002.

[11] W. Goodrich, Behavior of extended shear tabs in stiffened beam-to-column web connections," M.Sc. Thesis, Vanderbilt University, Nashville, TN, 2005.

[12] K. Thomas, R.G. Driver, S.A. Oosterhof,, L. Callele, Full-scale tests of stabilized and unstabilized extended single-plate connections, Structures, 10 (2017), pp.49-58.

[13] M. Mahamid, A. Rahman, A. Ghorbanpoor, The analyses of extended shear tab steel connections part II: stiffened connections, Eng. J. AISC, 44 (2) (2007), pp. 133-146.

[14] P.J. Fortney, W.A. Thornton, Analysis and design of stabilizer plates in single-plate shear connections, Eng. J. AISC, 53 (1) (2016), pp. 1-28.

[15] M. Marosi, Behaviour of single and double row bolted shear tab connections and weld retrofits," Master's Thesis, McGill University, Montreal, QC, 2011.

[16] M. Marosi, M. D'Aronco, R. Tremblay, C.A. Rogers, Multi-row bolted beam-to-column shear tab connections, 6th European Conference on Steel and Composite Structures, Budapest (2011).

[17] M. D'Aronco, Behaviour of double and triple vertical rows of bolts shear tab connections and weld retrofits," Master's Thesis, École Polytechnique de Montréal, Montreal, QC, 2013.

[18] A. Mirzaei, Steel shear tab connections subjected to combined shear and axial forces, PhD Thesis, McGill University, Montreal, QC, 2014.

[19] J. Hertz, Testing of extended shear tab connections subjected to shear, Master's Thesis, McGill University, Montreal, QC, 2014.

617 [20] N. Goldstein Apt, Testing of extended shear tab and coped beam-to-girder connections subject
618 to shear loading, Master's Thesis, McGill University, Montreal, QC, 2015.
619 [21] J. Hertz, D.G. Lignos, C.A. Rogers, Full scale testing of extended beam-to-column and Beam-
620 to-girder shear tab connections subjected to shear, 8th International Conference on Behavior of Steel
621 Structures in Seismic Areas, Shanghai (2015).
622 [22] CSA-S16-14, Limit States Design of Steel Structures, Canadian Standards Association,
623 Toronto, ON, 2014.
624 [23] ASTM A992 / A992M-11(2015), Standard Specification for Structural Steel Shapes, ASTM
625 International, West Conshohocken, PA, 2015.
626 [24] ASTM A572 / A572M-15, Standard Specification for High-Strength Low-Alloy Columbium-
627 Vanadium Structural Steel, ASTM International, West Conshohocken, PA, 2015.
628 [25] ASTM F3125 / F3125M-15a, Standard Specification for High Strength Structural Bolts, Steel
629 and Alloy Steel, Heat Treated, 120 ksi (830 MPa) and 150 ksi (1040 MPa) Minimum Tensile
630 Strength, Inch and Metric Dimensions, ASTM International, West Conshohocken, PA, 2015.
631 [26] A. Astaneh-Asl, K.M. McMullin, S.M. Call, Behavior and design of steel single plate shear
632 connections, J. Struct. Eng. ASCE, 119 (8) (1993), pp. 2421-2440.
633 [27] AISC 341-16, Seismic Provisions for Structural Steel Buildings, American Institute of Steel
634 Construction, Chicago, IL, 2016.
635 [28] G.L. Kulak, J.W. Fisher, H.A. Struik, Guide to design criteria for bolted and riveted joints, 2nd
636 Edition. American Institute of Steel Construction, Chicago, IL, 2001.
637 [29] I.R. Gomez, A.M. Kanvinde, Y.K. Kwan, G.Y. Grondin,Strength and ductility of fillet welds
638 subjected to out of plane bending, American Institute of Steel Construction, Chicago, IL, 2008.

639 [30] ASTM A6/A6M-04b, Standard specification for general requirements for rolled structural steel
640 bars, plates, shapes, and sheet piling, American Society for Testing and Materials, West
641 Conshohocken, PA, 2004.
642 [31] CSA-G40.20-13/G40.21-13, General requirements for rolled or welded structural quality steel/
643 structural quality steel, Canadian Standards Association, Toronto, ON, 2013.
644 [32] CISC, Handbook of steel construction, 11th edition, Canadian Institute of Steel Construction,
645 Markham, ON, 2016.
646 [33] A. Elkady, D.G. Lignos, Analytical investigation of the cyclic behavior and plastic hinge
647 formation in deep wide-flange steel beam-columns, Bull. Earthq. Eng., 13 (4) (2015), pp. 1097-1118.
648 [34] H. Daneshvar, One-sided steel shear connections in column removal scenario," P.h.D Thesis,
649 University of Alberta, Edmonton, AL, 2013.
650 [35] J.J Wallaert, J.W. Fisher, The shear strength of high-strength bolts, Lehigh University,
651 Bethlehem, PA,1964.
652 [36] J.J Wallaert, J.W. Fisher. Shear strength of high-strength bolts, J. Struct. Div. ASCE, 91 (3)
653 (1965), pp. 99-126.
654